




GRANT AGREEMENT No.: 764902		
Project Acronym: TOMOCON		
Project title: Smart tomographic sensors for advanced industrial process control		
Deliverable Rel. No. D4.2.	Lead Beneficiary ULIB	
EU Del. No. D13	Type Report	
WP No. WP4	Date: 22.08.2019	Revision: 0
Innovative Training Network TOMOCON		
Deliverable Title <div style="text-align: center; margin-top: 100px;"> Virtual Controller Structures for TOMOCON Demonstrations </div>		
Description <p>This report describes the controller structures, their models and numerical implementation for the TOMOCON virtual demonstrations.</p>		

Prepared by:	Dr. Jaroslav Hlava	
Approved by:	Prof. Dr. Uwe Hampel	
Approved by Supervisory Board:	06.09.2019	

Dissemination Level: **Public**



This project has received funding from the European Union's Horizon 2020 research and innovation programme under the Marie Skłodowska-Curie Grant Agreement No. 764902.

TOMOCON				GRANT AGREEMENT No.: 764902	
Deliverable Title: Virtual Controller Structures for TOMOCON Demonstrations					
Del. Rel. No.	EU Del. No.	WP No.	Lead Beneficiary	Type	Date
D4.2.	D13	WP4	ULIB	Report	22.08.2019

Revision Sheet

Revision Number	Purpose of Revision	Effective Date
0	Initial Issue	06.09.2019



TOMOCON				GRANT AGREEMENT No.: 764902	
Deliverable Title: Virtual Controller Structures for TOMOCON Demonstrations					
Del. Rel. No.	EU Del. No.	WP No.	Lead Beneficiary	Type	Date
D4.2.	D13	WP4	ULIB	Report	22.08.2019

Table of Contents

1. Introduction	4
2. Demonstration process: Inline swirl flow separator	5
2.1. Introduction	5
2.2. Process model.....	6
2.2.2. Control loop	10
2.2.3. Results.....	12
2.3. Conclusions and next steps	13
3. Demonstration process: Continuous casting	15
3.1. Introduction	15
3.2. Virtual controller structure for jet flow angle	15
3.2.1. Process model.....	16
3.2.2. Model predictive control.....	16
3.2.3. Virtual controller implementation	17
3.3. Virtual controller structure for meniscus velocity	19
3.3.1. Process model.....	19
3.3.2. Adaptive model predictive control	20
3.3.3. Virtual controller implementation	21
4. Demonstration process: Microwave drying.....	24
4.1. Introduction	24
4.2. State estimation	24
4.3. Controller design.....	25
4.4. Controller formulation.....	26
5. Demonstration process: Batch crystallization	28
5.1. Introduction	28
5.2. Physical and computational model	28
5.3. Tomographic output data in PID controller design	30
5.4. Case study	31
5.5. Conclusion and future work.....	32
6. Conclusion	33
7. References.....	35



TOMOCON				GRANT AGREEMENT No.: 764902	
Deliverable Title: Virtual Controller Structures for TOMOCON Demonstrations					
Del. Rel. No.	EU Del. No.	WP No.	Lead Beneficiary	Type	Date
D4.2.	D13	WP4	ULIB	Report	22.08.2019

1. Introduction

The utilization of process tomography in automatic control is still a very recent development in the field of control. Tomography sensors allow us to obtain rich multi-dimensional information about various industrial processes, rather than the traditional pointwise information that is obtained through more conventional sensors. However, there still remains the question of how do we utilize this rich multi-dimensional information. How can this information be processed in real time for the controller to take the required actions in the needed time? In the end, it becomes more than clear how big challenges arise when conventional control techniques are to be applied for these distributed parameter systems (DPS).

In this report, we introduce the preliminary structures for the controllers in each demonstration, and numerical implementations for the virtual demonstrations. One of the key steps needed for the controller structure is the process model. The report will show the different methodologies used to create the process model for the controller design, and how these models will be utilized in the controller structures.



TOMOCON				GRANT AGREEMENT No.: 764902	
Deliverable Title: Virtual Controller Structures for TOMOCON Demonstrations					
Del. Rel. No.	EU Del. No.	WP No.	Lead Beneficiary	Type	Date
D4.2.	D13	WP4	ULIB	Report	22.08.2019

2. Demonstration process: Inline swirl flow separator

2.1. Introduction

This text documents the current strategy of controlling the separation process in an inline swirl flow separator. To introduce the experimental system, a schematic of the swirl pipe region is presented in Figure 1.

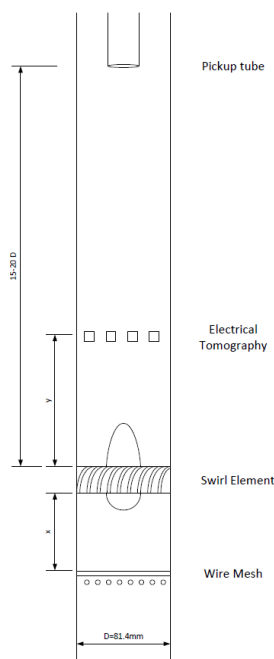


Fig. 1 Swirl pipe schematics

The domain of interest corresponds to the region between the electrical tomography sensor, and the pickup tube location. As a consequence, the generation of swirl motion and its profile are completely based on the CFD simulations (DNS) done within the framework of this project. The current fluid-dynamics modelling of the process assumes a dispersed phase with a one-way coupling between the phases, i.e., the particles have their trajectories affected by the surrounding fluid, however, no additional terms are considered in the Navier-Stokes equation to represent the forces of the particles in the fluid. As a consequence, the fluid is assumed to follow a single phase flow distribution.

The control strategy is based on an area factor that represents the opening of the two valves located at the outlets of the swirl pipe. A model to represent the effect of the valves was developed based on the flow over a step, however, no validation of the approach was provided so far. Several parameters can be changed during the simulation (bulk velocity, particle size, etc.), however, it is assumed in the process that only the distribution of the dispersed elements, adopted as an equivalent core radius, has quick changes in time (the other variables are assumed as quasi-steady state). The choice of an equivalent core radius is due to an easy extension to the gas core diameter for a further two-fluid model, currently

TOMOCON				GRANT AGREEMENT No.: 764902	
Deliverable Title: Virtual Controller Structures for TOMOCON Demonstrations					
Del. Rel. No.	EU Del. No.	WP No.	Lead Beneficiary	Type	Date
D4.2.	D13	WP4	ULIB	Report	22.08.2019

under development. The control is made at this point via a proportional-integral-derivative (PID) controller. The equivalent radius of distribution of particles is used as a control variable. Its value is measured after the swirl element by the Electrical Tomography sensor, and extrapolated to the pickup tube location via the fluid dynamics model of the process. There, the value is adopted as reference to adjust the valve opening parameter, to ensure that all the light phase is being captured at the central outlet while minimizing the amount of the continuous phase. This report resumes an initial approach to control the flow. Further improvements are listed in the conclusion section, and they are expected to be developed in the following months of the project.

2.2. Process model

2.2.1.1. Tangential velocity profile

The particle motion is highly influenced by the centripetal force caused by the flow rotation. The centripetal force scales with the velocity squared. Therefore, a proper approximation of the tangential velocity profile is fundamental to correctly predict the particle motion. The simulated velocity profile for a small Reynolds number ($Re = 4600$) follows in Figure 2. The figure indicates that the position of maximum angular velocity happens at $r \approx 0.6 R$ close to the swirl element. The position of the maximum velocity tends to close in the axial direction, and a region of decaying angular velocity seems to be formed after an entrance length of $2 D$. It is also notable that the solid body type of motion close to the center of the pipe. At this point it is interesting to emphasize that $Re = 4600$ corresponds to an axial velocity of 0.05m/s, which is considerable small in relation to the expected values of around 1m/s in the current setup. For higher Reynolds numbers the wall region present in Figure 2 tends to be squeezed towards the wall of the pipe.

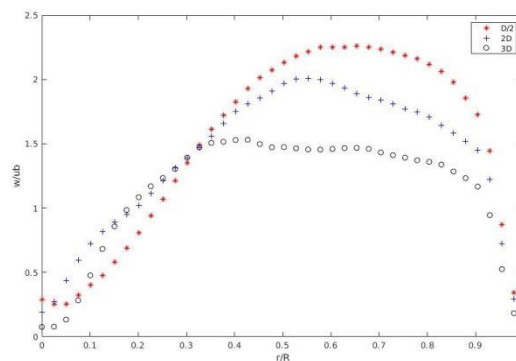


Fig. 2 Azimuthal velocity profile obtained by DNS simulations

Swirl number estimative

The swirl number at the inlet of the swirl pipe can be estimated at the inlet by calculating the flux of angular momentum leaving the swirl element. The axial velocity inside the vanes of the swirl element is proportional to the flow bulk velocity, with the constant of proportionality being the ratio between the pipe area and the free area of the element (mass conservation). The body diameter corresponds to 80% of the pipe diameter, generating an area ratio of around 3 ($v_z = 3 u_b$) for the current swirl elements. The vanes guide the flow

TOMOCON				GRANT AGREEMENT No.: 764902	
Deliverable Title: Virtual Controller Structures for TOMOCON Demonstrations					
Del. Rel. No.	EU Del. No.	WP No.	Lead Beneficiary	Type	Date
D4.2.	D13	WP4	ULIB	Report	22.08.2019

generating the tangential motion. Due to the impermeable characteristic of the vanes, the flow is forced to follow a path parallel to the walls. Therefore, the angular velocity is proportional to the tangent of the vane angle: $v_\theta = v_z \tan(\theta) = 3 u_b \tan(\theta)$. By assuming a conservation of angular momentum, the swirl number inside the swirl pipe is approximated to:

$$\Omega = \frac{1}{\pi u_b^2 R^3} \dot{L} = 6 (1 - 0.8^3) \tan(\theta) \approx 3 \tan(\theta) \quad (1)$$

2.2.1.2. Valve modeling

The valve model described as follows was inspired in the flow over a forward-facing step. Two recirculation zones are formed when a forward-facing step is present; one before the step and one after it. Figure 3 presents a sketch of the streamlines of a flow over a step. The size of the recirculation zone I varies little from case to case, but the size of the recirculation zone II is highly dependent on the size of the boundary layer thickness in relation to the step size (Sherry et al., 2010) (Ren et al., 2011).

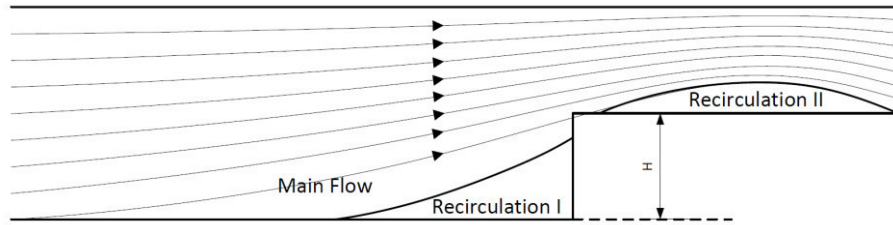


Fig. 3 Schematics of the streamlines of a flow over a forward-facing step

Two references (Bullen et al., 1996) and (Ando et al., 2004) regarding measurements in pipe contractions, both considering a turbulent flow, were used to model the valves. Bullen et al. focused on the results obtained for $Re = 1.54 \times 10^5$ with a diameter ratio between the pipes of 0.576. The authors obtained a full developed flow between $z = -4D_1$ and $z = -2D_1$, with an intact centerline velocity until $z = -D_1$. The vena contract location (region of maximum height of the Recirculation zone II) was estimated to occur at $z = 0.2D_1$, and reduces the region to 67% of the small pipe area. The valve model here developed assumes that the streamline separating the recirculation region and the flow region involves an area of the pipe given by a third order polynomial. The edge point was considered instead of the area ratio value at the *vena contracta* due to a further extension to different valve openings. Then, the polynomial is given by:

$$\frac{A}{A_t}(z) = \frac{10}{52} \left(1 - \frac{D_2^2}{D_1^2}\right) \left[\left(\frac{z}{D_1}\right)^3 + 2.7 \left(\frac{z}{D_1}\right)^2 - 1.2 \left(\frac{z}{D_1}\right) \right] + \frac{D_2^2}{D_1^2} \quad (2)$$

The above expression can be seen as a deviation of the pickup tube area given by the polynomial term. The extension to different valve openings (instead of a contraction) is made by multiplying the deviation of the pickup tube area term by a factor:

$$\frac{A}{A_t}(z) = \Phi \frac{10}{52} \left(1 - \frac{D_2^2}{D_1^2}\right) \left[\left(\frac{z}{D_1}\right)^3 + 2.7 \left(\frac{z}{D_1}\right)^2 - 1.2 \left(\frac{z}{D_1}\right) \right] + \frac{D_2^2}{D_1^2} \quad (3)$$

This factor is a function of both the valve openings. The polynomial term vanishes if $\Phi = 0$, indicating a parallel streamline connecting the unaffected region ($z < -2D$) and the affected one. If $\Phi = 1$, the previous solution for a pipe contraction is recovered, indicating

TOMOCON				GRANT AGREEMENT No.: 764902	
Deliverable Title: Virtual Controller Structures for TOMOCON Demonstrations					
Del. Rel. No.	EU Del. No.	WP No.	Lead Beneficiary	Type	Date
D4.2.	D13	WP4	ULIB	Report	22.08.2019

that the valve at the outer pipe acts as a pipe contraction. If $\Phi = \left(1 - \frac{D_1^2}{D_2^2}\right)^{-1}$ the area is zero, indicating that the valve at the pickup tube acts as a step. Note that it is assumed that the behavior of closing the center of the pipe is analogous to the behavior of closing an annular region, which may not be realistic. A plot of the stream line radial position and its area for $D_1 = 2D_2$ are presented in Figure 4.

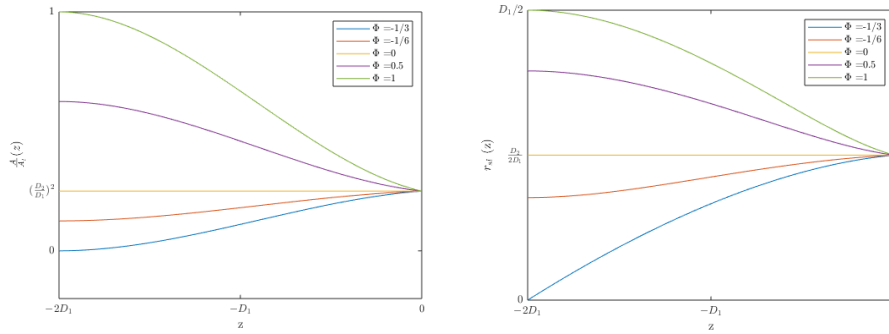


Fig. 4 Separating streamline area (left) and radial location (right) as a function of the valve opening factor and position

The streamlines are parallel to the flow velocity, isolating regions of constant volumetric flow rate. As a consequence, the flow split is determined at $z = -2 D_1$, for every instant of time.

2.2.1.3. 1D Navier Stokes equations

2.2.1.3.1. Unaffected region

The 1D integral balances are solved to model the flow in the problem. The simplification to a 1D model is required to reduce the complexity of equations, allowing a real time solution of the flow. The mass and angular momentum are the relevant quantities for the current approach. Their integral balances are given by:

$$\frac{\partial}{\partial t} \int_0^R r dr + \frac{\partial}{\partial z} \int_0^R v_z r dr = 0 \quad (4)$$

$$\frac{\partial}{\partial t} \int_0^R \rho v_\theta r^2 dr + \frac{\partial}{\partial z} \int_0^R \rho v_z v_\theta r^2 dr = \tau_{r\theta}(R) R^2 \quad (5)$$

The time dependent terms are negligible far from the valve due to the flow quasi-steady state hypothesis. However, close to the element, due to the constant changes in the projected area of the outlets (by the valve model), the flow has to be accelerated, and the time dependent terms are important.

2.2.1.3.2. Valve-affected region

Due to the high accelerations inside the region affected by the valve, a separated model is developed for the location. The valve model previously explained determines the position of a streamline separating the flows going to the pickup tube and to the outer pipe. Focusing on the flow going to the light phase outlet (LPO) (the pickup tube), it is possible to write the balance of mass between the centerline and streamline as:

$$\frac{dm}{dt} = m_{in} - m_{out} \quad (6)$$

TOMOCON				GRANT AGREEMENT No.: 764902	
Deliverable Title: Virtual Controller Structures for TOMOCON Demonstrations					
Del. Rel. No.	EU Del. No.	WP No.	Lead Beneficiary	Type	Date
D4.2.	D13	WP4	ULIB	Report	22.08.2019

Where m is the mass of liquid contained between the centerline of the pipe and the streamline. The mass is given by the density of the liquid times the volume (no volume fraction correction, to account for the particles, is considered). At the same time, the mass flow rates can be written in terms of the areas and velocities:

$$m = \rho \int_{-2D}^0 A(z) dz \quad (7)$$

$$\dot{m}_{in} = \rho u_b A(-2D) \quad (8)$$

$$\dot{m}_{out} = \rho q_{lpo} \quad (9)$$

Then, applying the valve area equation from the previous sections leads to:

$$\Phi' \equiv \Phi \left(1 - \frac{D_2^2}{D_1^2} \right) + \frac{D_2^2}{D_1^2} \quad (10)$$

$$\pi \frac{D_1^3}{2} \frac{7}{13} \frac{d\Phi'}{dt} = u_b \pi \frac{D_1^2}{4} \Phi' - q_{lpo} \quad (11)$$

Note that Φ' is an indicative of the area of the flow that is captured by the LPO at the entrance of the valve affected region. $\Phi' = 0$ if no flow will cross the pickup tube, $\Phi' = D_2^2/D_1^2$ if the valves play no effect in the flow, and $\Phi' = 1$ if all the flow crosses the pickup tube. The streamline profile inside the valve affected region is used only to calculate the volume of liquid contained in the location, acting as a coefficient at the left side of the equation. This coefficient (currently given by 13/14) can be calibrated for different conditions.

$$\frac{d\Phi'}{dt} = \frac{13}{14D_1} \left[u_b \Phi' - \frac{q_{lpo}}{A_p} \right] \quad (12)$$

Note that the change in the volume is dependent on the difference between the flow rate entering and leaving the region. As a consequence, the controller acts in the flow rate leaving the region to generate the desired change of position of the streamline as a function of time. Introducing the Flow split, given by the ratio between the flow leaving the pickup tube and the total flow rate, the above expression can be re-written as:

$$\frac{d\Phi'}{dt} = \frac{13u_b}{14D_1} [\Phi' - FS] \quad (13)$$

The above equation is used for the control step.

2.2.1.4. Particle tracking

The particles are injected at the inlet, and their position at the entrance of the valve affected region is used as a reference for the control step. The choice of the beginning of the valve affected location is justified by the swirl decay and by the small length of the region. Because of the swirl decay, the angular velocity is always smaller at the location than at the inlet. Therefore, the radial velocity is also smaller. This effect, aligned with the small length of the section, results in a small change of the radial position of the particle along the axial direction. Note that the swirl motion always forces the particles to the center of the pipe if they are lighter than the continuous phase. Also, due to the separating streamline, no liquid flow can cross the separated regions. Therefore, the approach results, in the worst case scenario, in a prediction of the radial position at the outlet larger than the real position of the particle. The approach impacts the efficiency, but at the same time ensures that the dispersed phase is always being captured if it is predicted as captured. The behavior is analogous for heavier particles in relation to the HPO.



TOMOCON				GRANT AGREEMENT No.: 764902	
Deliverable Title: Virtual Controller Structures for TOMOCON Demonstrations					
Del. Rel. No.	EU Del. No.	WP No.	Lead Beneficiary	Type	Date
D4.2.	D13	WP4	ULIB	Report	22.08.2019

Instead of tracking every particle crossing the pipe inlet, only the furthest particle (in relation to the centerline) is tracked. This is done to save the computational cost of a multiple particle tracking. The swirl motion generates a force always pointing against the radial direction, then, if the furthest particle is captured, all the intermediary ones are too. Note that this is only valid for a dispersed phase with a fixed diameter. The balance of forces in the radial direction is used to track the particle position over time. The forces considered in the model are the drag force, the centripetal acceleration and the virtual mass force:

$$\left(\rho_p + \frac{1}{2}\rho_c\right) \frac{dV_{p,r}}{dt} = \frac{(\rho_p - \rho_c)V_\theta^2}{r} + \frac{3C_d\rho_c(V_{c,r} - V_{p,r})|V_{c,r} - V_{p,r}|}{4\delta} \quad (14)$$

In the equation, the subscript “p” represents the particle and the subscript “c” represents the continuous phase. δ is the particle diameter. The current scenario works with a water flow as the continuous phase, with $v_c \approx 10^{-6} m^2/s$. For an estimative of the radial velocity, a pipe length of 2m and 10cm diameter is considered, with a bulk velocity of 2m/s. Then, a particle leaving the wall location at the inlet, and reaching the center of the pipe at the outlet, has $V_r = O(R u_b/L)$. As a consequence, the Stokes regime ($Re < 0.3$) is reached only if $\delta = O(10 \mu m)$ and the inertial regime is reached only if $\delta = O(1 cm)$. Then, it is assumed that the particles follow the transitional relation.

2.2.1.4.1. Particle position at the beginning of the valve – affected area

The control of the flow is given based on the particle position at $z = L - 2D$, where the valves are able to control the flow direction. The following procedure is used to obtain the particle radial position at the outlet:

- Calculate the core reaching position depending on the signal of k and on the initial position of the particle.
- If the core is not crossed before $L - 2D$, the non-crossing equations are employed based on the initial location.
- Otherwise, the position is achieved by setting $z_0 = z_c$ in the respective equations for the second part of the motion.

Because of the constant bulk velocity, the particle radial position at $z = L - 2D$ can be calculated as a function of time adopting:

$$r_p(L - 2D, t) = r_{p,calculated}(t - u_b(L - 2D)) \quad (15)$$

2.2.2. Control loop

Now that all the fluid dynamics part of the project has been described, it is possible to define our control loop. The control loop is built around the Φ' variable. The control is given based on the flow rate at the inner pipe, q_{lpo} . At this point the control is given by a PID loop, illustrated in Figure 5.



TOMOCON				GRANT AGREEMENT No.: 764902	
Deliverable Title: Virtual Controller Structures for TOMOCON Demonstrations					
Del. Rel. No.	EU Del. No.	WP No.	Lead Beneficiary	Type	Date
D4.2.	D13	WP4	ULIB	Report	22.08.2019

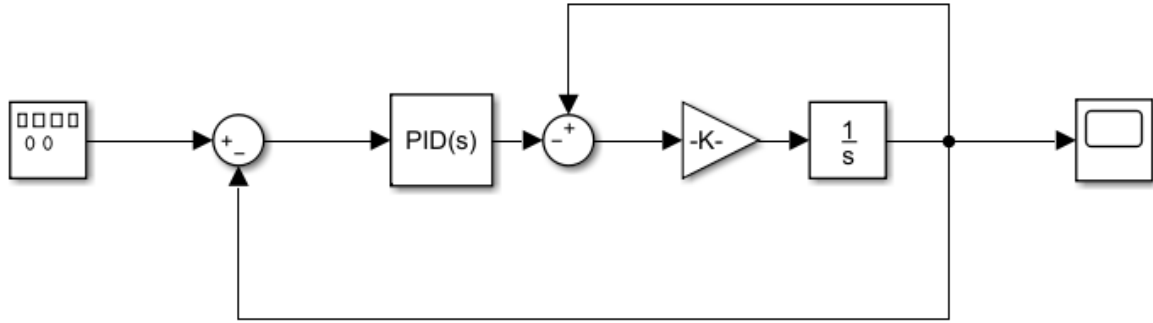


Fig. 5 Control loop currently adopted

2.2.2.1. Reference signal

Because of the assumption that the capturing is determined at the beginning of the valve-affected region, the reference for Φ' is proportional to the particle position at the location. The area inside the streamline separating the flow going through the pickup tube and the flow going to the outer pipe is given by:

$$\frac{A}{A_t}(L - 2D) = \Phi' \quad (16)$$

A particle at r_p/R at the location goes to the pickup tube if

$$\frac{A}{A_t} > \frac{r_p^2}{R^2} \quad (17)$$

As a simplification, it is adopted that the particles are always lighter than the continuous phase (and, therefore, captured at the pickup tube). Then, the reference for Φ' is given by:

$$\begin{aligned} ref(t) &= \kappa \frac{r_p^2}{R^2}(t) \\ &\text{with } \kappa > 1. \end{aligned} \quad (18)$$

2.2.2.2. Controller

A PID controller is adopted for the control step. The controller is responsible to set the Flow split, FS, in the equation describing the mass balance of the region contained by the streamline.

2.2.2.3. Control plant

As previously mentioned, the control plant is given by:

$$\frac{d\Phi'}{dt} = \frac{13u_b}{14D_1} [\Phi' - FS] \quad (19)$$

Note that Φ' is limited between 0 and 1 during the integration. In Figure 5, the constant multiplying both the FS and the current factor is represented by the gain.

TOMOCON				GRANT AGREEMENT No.: 764902	
Deliverable Title: Virtual Controller Structures for TOMOCON Demonstrations					
Del. Rel. No.	EU Del. No.	WP No.	Lead Beneficiary	Type	Date
D4.2.	D13	WP4	ULIB	Report	22.08.2019

2.2.3. Results

2.2.3.1. Constant inlet

The response of the system to the unitary step function was used to set the constants of the controller. The constants are given by:

$$K_p = -8$$

$$K_I = -50$$

$$K_d = 0.04$$

Also, a unitary filter coefficient for the derivative term is adopted. The response for the unitary step function without limiting the output is presented in Figure 6. Note that it takes around 0.5s for the valve to adjust the flow, which is around the time-scale of the real valves.

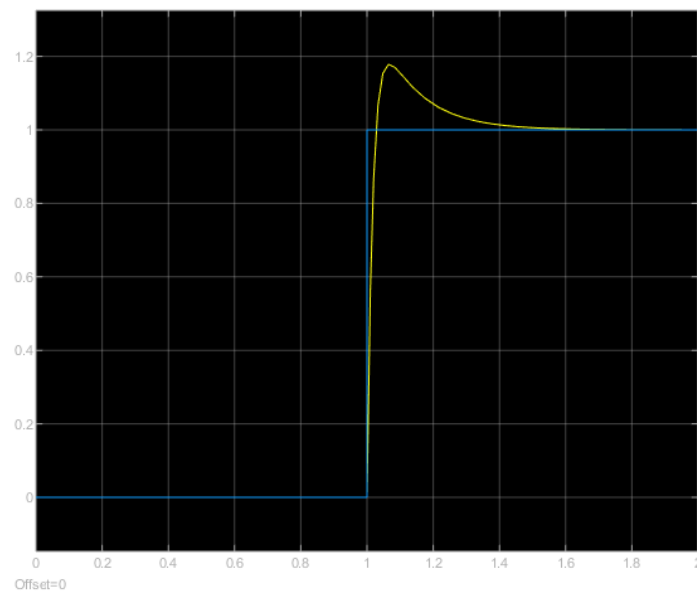


Fig. 6 Response to a unitary step inlet. Unlimited values.

2.2.3.2. Response to an oscillating reference

A sine function of frequency 10rad/s was adopted to check the response time of the controller to the disturbance. The response obtained is presented in Figure 7. Note that the peaks and valleys of the area fraction being captured by the valve are removed due to the physical limits of the value (set by the integral term – 1/s).



TOMOCON				GRANT AGREEMENT No.: 764902	
Deliverable Title: Virtual Controller Structures for TOMOCON Demonstrations					
Del. Rel. No.	EU Del. No.	WP No.	Lead Beneficiary	Type	Date
D4.2.	D13	WP4	ULIB	Report	22.08.2019

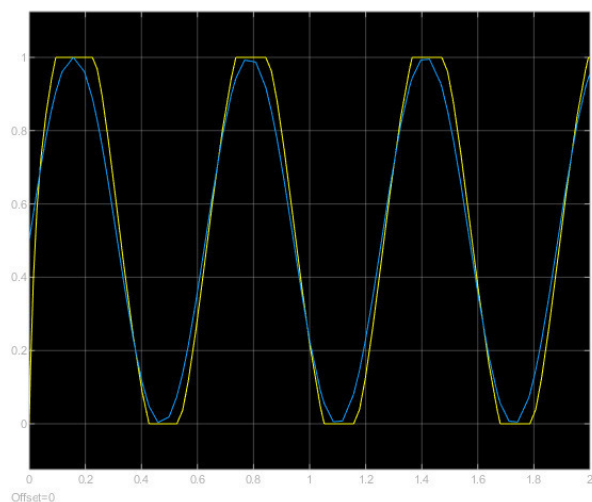


Fig. 7 Response to sine function

2.2.3.3. Response to a random inlet

The particle radial position arriving at the inlet of the valve-affected location is a random variable. Therefore, a random function was used to simulate the arrival of the particles at the location. The response for a random oscillating inlet is presented in Figure 8.

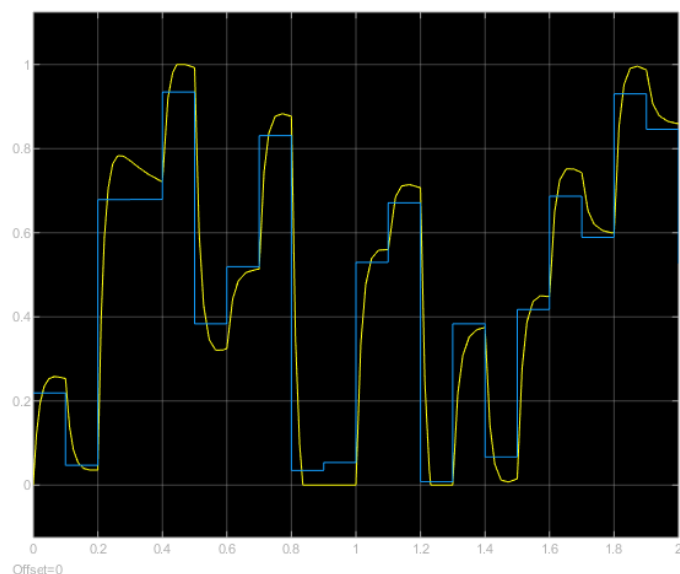


Fig. 8 Response to a random function

2.3. Conclusions and next steps

A dynamic model for the valve was successfully developed. The model was able to follow a random signal at the inlet of the valve-affected area. The next step before the virtual demonstration consists in including the calculation of the distribution of particles arriving at the inlet of the valve affected region as a function of time, by the methods described within

TOMOCON				GRANT AGREEMENT No.: 764902	
Deliverable Title: Virtual Controller Structures for TOMOCON Demonstrations					
Del. Rel. No.	EU Del. No.	WP No.	Lead Beneficiary	Type	Date
D4.2.	D13	WP4	ULIB	Report	22.08.2019

this document. The inlet of the demonstration will consist on the real measurements obtained by ESR10 Muhammad Awais Sattar and ESR1 Benjamin Sahovic. After the virtual demonstration the plan is to move towards a MPC, and to a deeper understanding of the physics of the flow, in order to remove part of the assumptions made in the current model. Also, a two-fluid model is being developed, which better represents the flow configuration inside the swirl pipe observed by the other ESRs in the project.



TOMOCON				GRANT AGREEMENT No.: 764902	
Deliverable Title: Virtual Controller Structures for TOMOCON Demonstrations					
Del. Rel. No.	EU Del. No.	WP No.	Lead Beneficiary	Type	Date
D4.2.	D13	WP4	ULIB	Report	22.08.2019

3. Demonstration process: Continuous casting

3.1. Introduction

The continuous casting process consists mainly of transforming liquid metal to solid metal. The process begins with the liquid metal flowing from a ladle to a 'tundish' which serves as a buffer vessel. The metal flows down through a Submerged Entry Nozzle (SEN) into a mould. The flow rate is there controlled by a stopper rod or a sliding gate. In the water cooled mould a thin solid shell on the metal surface is formed. The partly solidified strand is then continuously transported on rolls at a speed that matches the flow of the incoming metal and cooled by water sprays until it is solidified completely (Thomas, 2003). Due to the complex nature of the process, there are many variables that need to be considered when designing the controller structure. One of the main challenges in designing the controller is selecting the appropriate variables to control in order to achieve the optimum flow pattern needed in the mould to produce higher quality steel. The rest of the report will describe two controller structures designed for two separate manipulated variables; the exiting jet flow angle from the SEN, and the surface velocity of the mould.

3.2. Virtual controller structure for jet flow angle

The optimum flow pattern observed in the mould is a symmetric double roll flow as opposed to the single roll (see Figure 9). The double roll flow allows for the impurities to rise to the free surface and as a result decreases slug entrainment in the solid steel (Cukierski et al., 2007). The objective of the controller in this case will be to maintain the angle of the jet between the ranges of 10° to 15° to prevent deep jet impingement during the process, therefore avoiding the entrapment of slug and sustaining the double roll flow. The angle of the jet will be calculated from the velocity fields measured by the Contactless Inductive Flow Tomography (CIFT). The actuator used to change this angle is the varying magnetic field of the Electromagnetic Brake (EMBr).

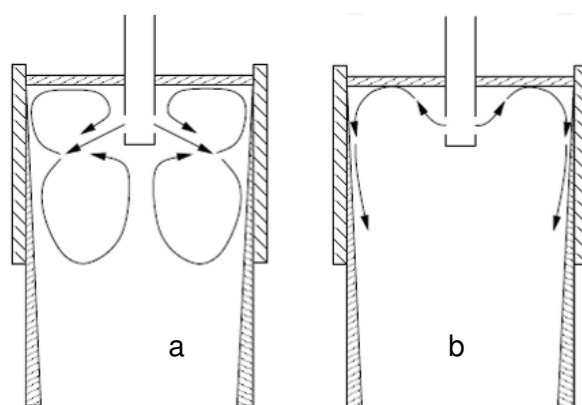


Fig. 9 a) Double roll flow pattern, b) Single roll flow pattern

TOMOCON				GRANT AGREEMENT No.: 764902	
Deliverable Title: Virtual Controller Structures for TOMOCON Demonstrations					
Del. Rel. No.	EU Del. No.	WP No.	Lead Beneficiary	Type	Date
D4.2.	D13	WP4	ULIB	Report	22.08.2019

3.2.1. Process model

A black-box model was created using data obtained from the Mini-LIMMCAST setup in HZDR. The data was obtained by varying the current going to the EMBr, and measuring the velocity fields in the mould during the experiments. The angle of the jet is derived from the measured velocity fields in the mould; in this case we assumed symmetry between both sides of the SEN, therefore only concentrating on half of the mould area. A model for the system was created using the System Identification Toolbox in MATLAB. Model input is the brake current, model output is the angle of the jet exiting the SEN. It turned out that the relationship between the brake current and jet angle can be described by a linear model in the form of the following first order transfer function

$$G(s) = \frac{-0.04429}{1.4443s+1} \quad (20)$$

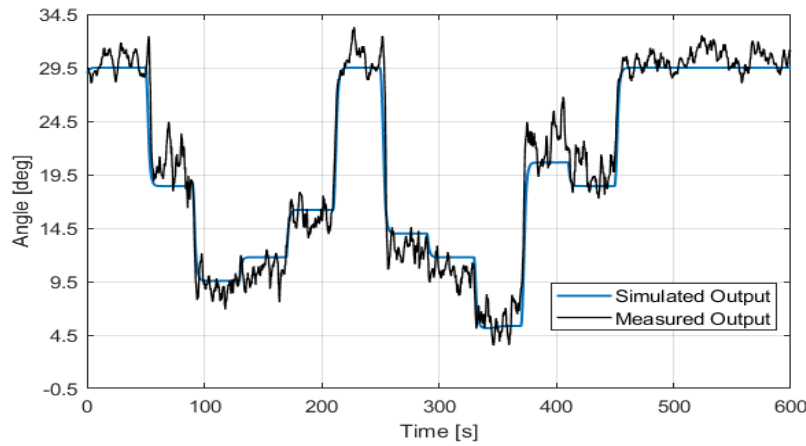


Fig. 10 Comparison of simulated model output with measured output

3.2.2. Model predictive control

The objective of the controller is to maintain the jet angle in the range between 10° and 15° during the operation of the casting process. Additionally, there are constraints on the input current to the electromagnetic brake. Due to the above reasons a controller based on Model Predictive Control was used in the control loop. MPC is known to outperform PID both in constraint handling and range control. The Model Predictive Control Toolbox in MATLAB was utilized for this step. The algorithm begins by converting the first order model into the below discrete time state space form:

$$x_p(k+1) = A_p x_p(k) + B S_i u_p(k) \quad (21)$$

$$y_p(k) = S_o^{-1} C x_p(k) + S_o^{-1} D S_i u_p(k) \quad (22)$$

Where A_p , B , C , D are the state-space matrices. S_i and S_o are the input and output scale factors. x_p is the state vector. u_p is the input variables. y_p is the output variables. A quadratic cost function is used for the optimization problem in order to determine the manipulated variable that should be applied in the future.

TOMOCON				GRANT AGREEMENT No.: 764902	
Deliverable Title: Virtual Controller Structures for TOMOCON Demonstrations					
Del. Rel. No.	EU Del. No.	WP No.	Lead Beneficiary	Type	Date
D4.2.	D13	WP4	ULIB	Report	22.08.2019

3.2.3. Virtual controller implementation

The virtual controller was implemented using MATLAB/Simulink as seen in Figure 11. Two sets of simulations were performed; the first simulation included set point tracking where we analysed the controller's response to various changes to the set point (see Figure 12 and 13), four different set points were used at intervals of $t=20s$ for this simulation. The controller was able to successfully track the set point with an average settling time of $t=5s$. The second set of simulations concentrated on disturbance rejection (see Figure 14 and 15) which is the main concentration of this study.

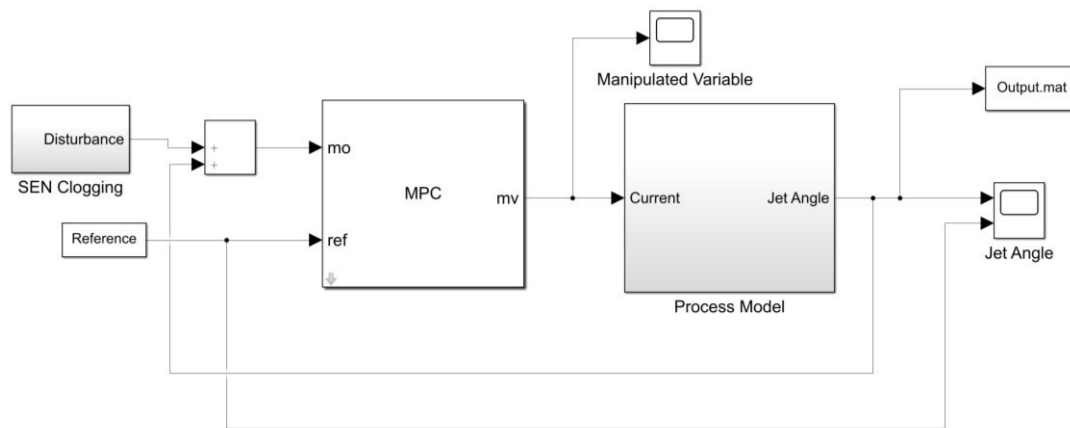


Fig. 11 Control loop implementation using Simulink

We introduce nozzle clogging as a disturbance to our process so that we can assess how efficient the controller is able to maintain the optimum angle range, while rejecting the disturbance produced by the nozzle clogging. We assumed that the clogging is occurring on the opposite side of the nozzle. Due to the blocked area on the one side of the nozzle, the flow exiting the opposite outlet is increased, which results in a deeper jet impingement in the mould as shown in (Cho et al., 2012). The clogging disturbance can be modelled as output disturbance because it directly changes the angle of the jet (Cho et al., 2012). The clogging and unclogging have different dynamics. Clogging of the nozzle occurs gradually with time; therefore, a ramp function should be used to simulate the increase in the jet angle. However, unclogging may be much faster. Typically, pieces of the clogged material break off into the flow in the mould and the effect is quite sudden. This can adequately be modelled as step disturbance. Both clogging and unclogging were simulated to see how the controller reacts to both situations.

Disturbance due to clogging was introduced at $t=20s$ (see Figure 14) which resulted in a gradual increase in the angle response. Furthermore, the effect of unclogging was also introduced at $t=50s$ which decreased the angle response. In both the clogging and unclogging disturbances, the MPC was able to respond quickly and reject the disturbances in order to maintain the set point reference. We avoided using a more aggressive control effort by the MPC as to avoid reaching saturation in the input control. Furthermore, we implemented open loop control which is generally used in industry, and compared it with our design for the closed loop control; Figure 14 shows that a closed loop system is needed to

TOMOCON				GRANT AGREEMENT No.: 764902	
Deliverable Title: Virtual Controller Structures for TOMOCON Demonstrations					
Del. Rel. No.	EU Del. No.	WP No.	Lead Beneficiary	Type	Date
D4.2.	D13	WP4	ULIB	Report	22.08.2019

prevent the angle from rapidly increasing, and therefore avoid a deeper jet impingement into the mould due to disturbances such as nozzle clogging.

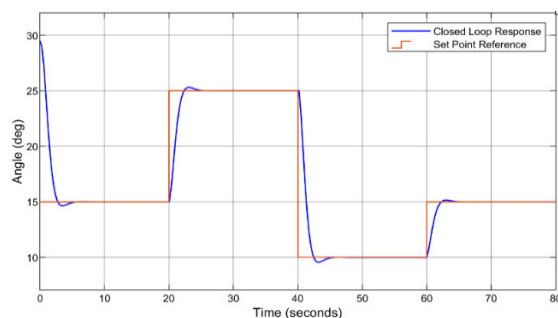


Fig. 12 Closed loop response for set point tracking

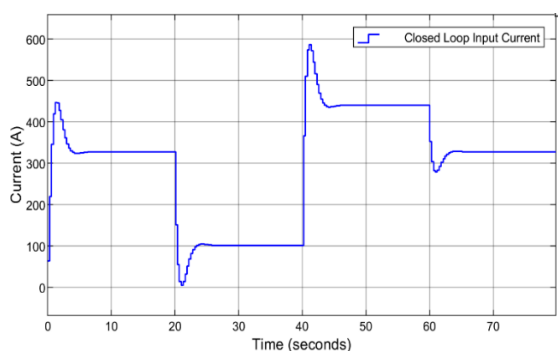


Fig. 13 Input current for set point tracking

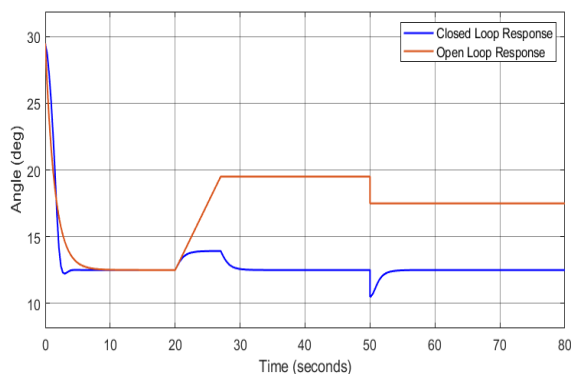


Fig. 14 Comparison of angle responses for disturbance rejection

TOMOCON				GRANT AGREEMENT No.: 764902	
Deliverable Title: Virtual Controller Structures for TOMOCON Demonstrations					
Del. Rel. No.	EU Del. No.	WP No.	Lead Beneficiary	Type	Date
D4.2.	D13	WP4	ULIB	Report	22.08.2019

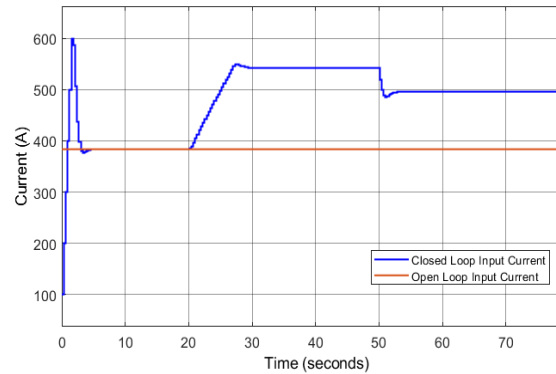


Fig. 15 Comparison of brake current during disturbance rejection

3.3. Virtual controller structure for meniscus velocity

Meniscus velocity refers to the surface velocity of the mould. Meniscus velocity needs to be kept between a specific range; too high velocities create excessive turbulences that can increase the potential of slug entrapment. On the other hand, too low meniscus velocities result in excessive cooling which can cause various surface defects as well (Liu, 2014). Furthermore, the meniscus velocity can help determine the various flow patterns that can occur in the mould (see Figure 9). The main objective of the controller is to maintain the meniscus velocity within the optimum range and to reject disturbances during the process. The meniscus velocity will be measured by the Contactless Inductive Flow Tomography (CIFT).

3.3.1. Process model

A dynamic neural network with feedback connections was used for the nonlinear autoregressive model with exogenous inputs (NARX). The NARX model is based on the linear ARX model but instead of using the weighted sum of its regressors to predict the current output, it uses a nonlinear mapping function f as can be seen in equation 23. In our case the nonlinearity estimator will be done using the neural network in Figure 16. The neural network time series toolbox in MATLAB was used to design the model.

$$y(t) = f(y(t-1), y(t-2), \dots, y(t-n_y), u(t), u(t-1), u(t-2), \dots, u(t-n_u)) \quad (23)$$

The NARX network consists of a two-layered feedforward network. A sigmoid function is used in the hidden layer, while a linear transfer function is used in the output layer. The tapped delay line allows for previous input and output values to be stored. The input $x(t)$ represents the current going to the EMBR, while the output $y(t)$ represents the meniscus velocity. It is clear that a feedback connection is needed for the network to take in previous values of the meniscus velocity in order to create the dynamic model. In our case ten hidden neurons were used, with the number of delays of two.

TOMOCON				GRANT AGREEMENT No.: 764902	
Deliverable Title: Virtual Controller Structures for TOMOCON Demonstrations					
Del. Rel. No.	EU Del. No.	WP No.	Lead Beneficiary	Type	Date
D4.2.	D13	WP4	ULIB	Report	22.08.2019

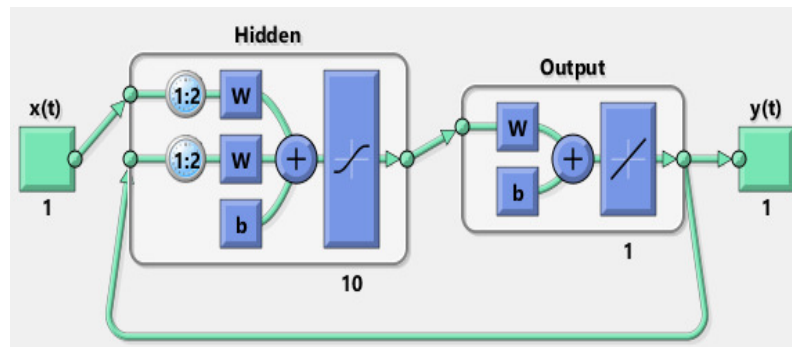


Fig. 16 Neural network NARX model

Figure 17 compares the output of the NARX neural network model with the measured velocities from the random current input experiment. The model is able to track the changes in meniscus velocity without overfitting the data; however it can be seen that the performance of the network can further be improved.

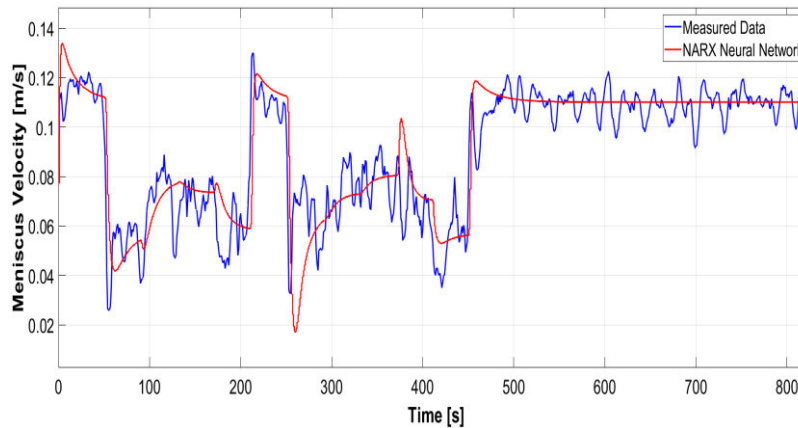


Fig. 17 Comparison of neural network output with experimental data

3.3.2. Adaptive model predictive control

The main objective of the controller is to maintain the meniscus velocity within the optimum range and to reject disturbances during the process. Besides minimum and maximum limits related to the optimum range of the meniscus velocity, there is also the maximum limit on the current of the EMBR. Hence Model Predictive Control (MPC) is a natural choice due to its excellent constraints handling ability. As it is evident from the previous section, the controlled plant is not only nonlinear but there are other issues as well. This nonlinearity is not well amenable to analytic description and it may be time varying. This would complicate the use of nonlinear MPC. We also regarded it as desirable to keep the beneficial features of MPC based on linear models and quadratic programming. For all of these reasons our approach of choice is to implement adaptive MPC where online model estimation is used to update the internal plant model in order to achieve a reasonable level of control performance with this nonlinear plant. The following constraints will be applied during the process:

TOMOCON				GRANT AGREEMENT No.: 764902	
Deliverable Title: Virtual Controller Structures for TOMOCON Demonstrations					
Del. Rel. No.	EU Del. No.	WP No.	Lead Beneficiary	Type	Date
D4.2.	D13	WP4	ULIB	Report	22.08.2019

$$0 \leq u(k + i - 1) \leq 600 \quad (24)$$

$$0.06 \leq y(k + i - 1) \leq 0.08 \quad (25)$$

for all $i = \{1, N\}$

3.3.3. Virtual controller implementation

The virtual controller was implemented using MATLAB/Simulink as seen in Figure 18. This adaptive MPC is based on a continuously updated linearized model. For this purpose, NARX Neural network is linearized and converted to the discrete time state space form. The “Recursive Polynomial Model Estimator” block estimates a discrete time ARX model based on the input (current to EMBR) and output (meniscus velocity) from the Neural Network. The model is converted into state space form using the block “Model Type Converter”. The Adaptive MPC updates its internal plant model using the output from the “Model Type Converter” at each control interval, therefore the controller can adapt its internal prediction model for changing operating conditions.

The first set of simulations concentrates on set-point tracking where the controller’s response to various changes to the set point is analyzed (see Figure 19 and 20), four different set points were used. The controller was able to successfully track the set point with the settling time ranging from 50 to 100s. It is important to note that at the beginning of the simulation the Recursive Polynomial Model Estimator needs time to reach an adequate model. This explains the oscillatory behaviour from 0 to 400s. In this case the constraints on the manipulated variable are applied after this period to allow the model estimator to reach an adequate model.



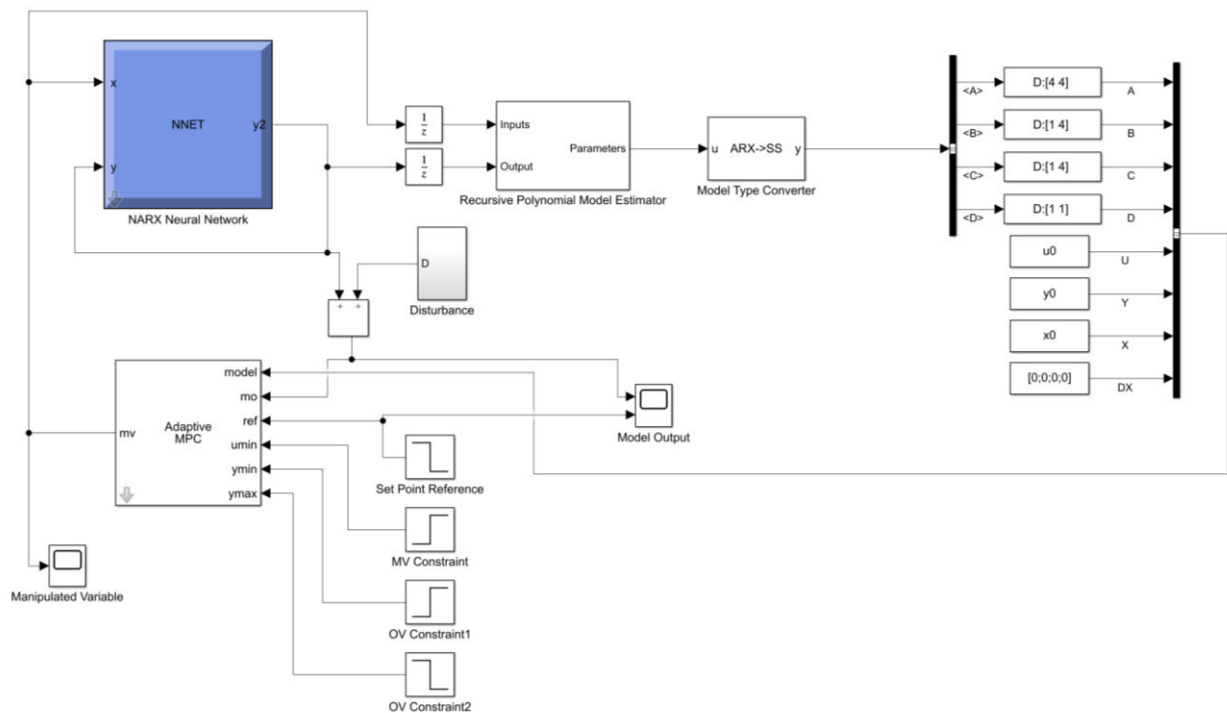


Fig. 18 Control loop implementation using Simulink

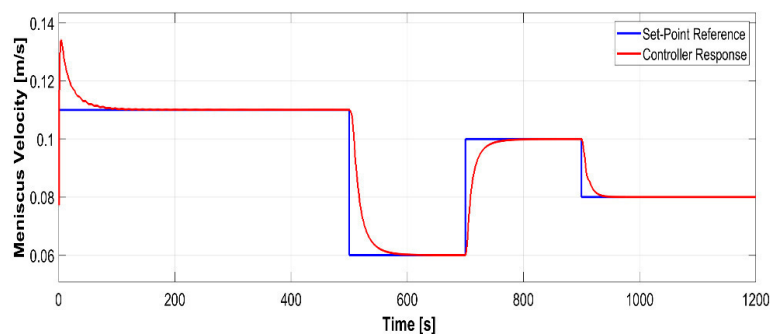


Fig. 19 Closed loop response for set point tracking

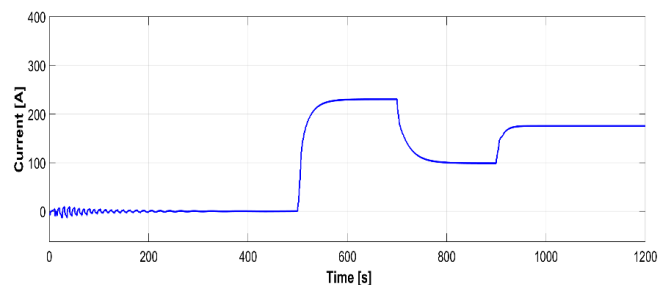


Fig. 20 Input current for set point tracking

The second set of simulations concentrates on disturbance rejection (see Figure 21 and 22) which is the main objective of the controller. One of the main disturbances in the

TOMOCON				GRANT AGREEMENT No.: 764902	
Deliverable Title: Virtual Controller Structures for TOMOCON Demonstrations					
Del. Rel. No.	EU Del. No.	WP No.	Lead Beneficiary	Type	Date
D4.2.	D13	WP4	ULIB	Report	22.08.2019

continuous casting process is the changing of the casting speed. The casting speed is changed sporadically throughout the process; it would be valuable to see if an automatic control loop can keep the meniscus velocity in the optimum range and reject the effect that might occur from changing the casting speed. The optimum range for the meniscus velocity in the Mini-LIMMCAST setup is between 0.06 to 0.08 m/s. The disturbance from changing the casting speed will be applied at the output of the model; increasing the casting speed results in an increase in the meniscus velocity. The effect of the disturbance on the velocity will be taken from (Liu, 2014) where the casting speed of the continuous caster at ArcelorMittal Dofasco was varied, and the meniscus velocity at the midpoint between the mould wall and the SEN was measured during the changes. The meniscus velocity was measured using an SVC sensor and the nail board method. Figure 21 shows that the controller was able to maintain the optimum range for the velocity. Figure 22 shows that the controller does not exceed the constraints applied during the process.

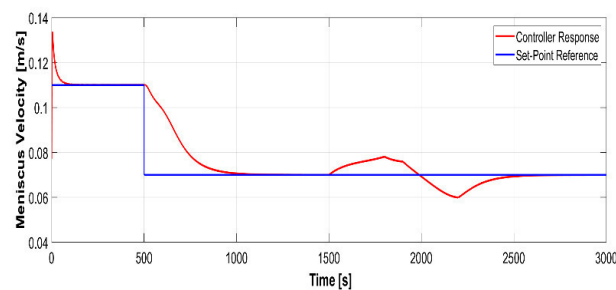


Fig. 21 Closed loop response for disturbance rejection

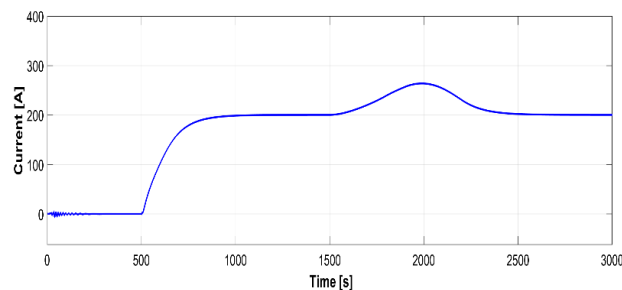


Fig. 22 Input current for disturbance rejection



TOMOCON				GRANT AGREEMENT No.: 764902	
Deliverable Title: Virtual Controller Structures for TOMOCON Demonstrations					
Del. Rel. No.	EU Del. No.	WP No.	Lead Beneficiary	Type	Date
D4.2.	D13	WP4	ULIB	Report	22.08.2019

4. Demonstration process: Microwave drying

4.1. Introduction

Drying of dielectric materials is one of the common processes in several industries. Among the main objectives of this process are adjusting the non-uniform moisture distribution of the target and reduction of energy consumption and processing time. Microwave heating technology makes the volumetric and selective heating possible. To benefit from its features, an advanced control system should be developed for distributed microwave sources. However, moisture distribution information and a process model are required to derive this controller. Figure 23 shows the closed-loop of this process.

The controller receives moisture information of an impregnated foam from the sensors, either Electrical Capacitance Tomography (ECT) or Microwave Tomography (MWT), compares it to the desired moisture level and calculates the command power level for each microwave source individually.

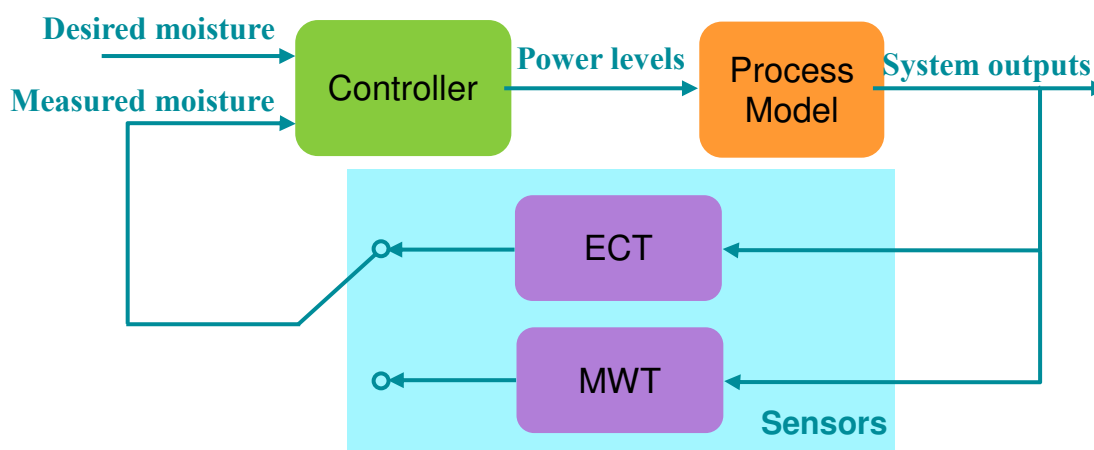


Fig. 23 Microwave drying process closed loop

Three different controllers have been selected as candidates for this task: Linear Quadratic Gaussian (LQG) controller, Model Predictive Controller (MPC) and neural network controller. The first and the second one need an analytical process model while using the third controller we can benefit from a black-box model. By comparing the performance of these controllers, the best one will be chosen to be implemented in the final demonstration.

4.2. State estimation

In the drying procedure, the foam passes through a cavity. While the foam is inside the cavity, its moisture information cannot be measured and only the moisture information of the foam portion outside the cavity is available. Therefore, we need to estimate the process states by an observer to work with the controller. Among different kinds of observers, the Kalman filter is a suitable choice because of its simple yet effective structure. We intend to use this filter to estimate the moisture content of the foam portion inside the cavity.

TOMOCON				GRANT AGREEMENT No.: 764902	
Deliverable Title: Virtual Controller Structures for TOMOCON Demonstrations					
Del. Rel. No.	EU Del. No.	WP No.	Lead Beneficiary	Type	Date
D4.2.	D13	WP4	ULIB	Report	22.08.2019

4.3. Controller design

The choice of the candidate controllers is based on their features and the process properties and constraints. At the current state, the LQG controller has been studied and investigated to design the multi-input multi-output controller of the microwave drying process. This method is a linear control method and is the combination of the Linear Quadratic Regulator (LQR) controller and the Kalman filter. In this method, the computations are done just once and the controller will be a constant gain matrix, so the computation and implementation costs are low. This method also benefits from a Kalman filter which, as already been mentioned in the previous section, is a requirement due to the lack of information.

The LQG controller is a stabilizing controller which means using this controller, the system states will converge to their equilibrium point. However, the control objective in the microwave drying process is to track the desired setpoint for the moisture content. One approach to achieve this goal is to use an integral action together with the LQG controller. Figure 24 shows the LQG controller structure with integral action.

The system outputs which are the moisture and the temperature of the foam are measured by the sensors. They are, however, measured only at some parts of the foam. The system input and output data are then given to the Kalman filter to estimate all the system states. The system states include both moisture and temperature of the foam. The temperature at the surface of the foam in this demonstration is measured by an already installed infrared camera. In this diagram, we do not emphasize the temperature information since it is available also inside the cavity and it is not the control objective. However, it will be used by the controller. In a regular LQG, the estimated states by the Kalman filter will be applied to the LQR controller. Nonetheless, there is one more step before that in this form of the controller. The measured moisture is compared with the setpoint and an augmented state vector including the system states and the integral of tracking error is fed to the LQR controller. The LQR controller then derives the augmented states including the tracking errors to zero which means the system outputs will track the setpoint.

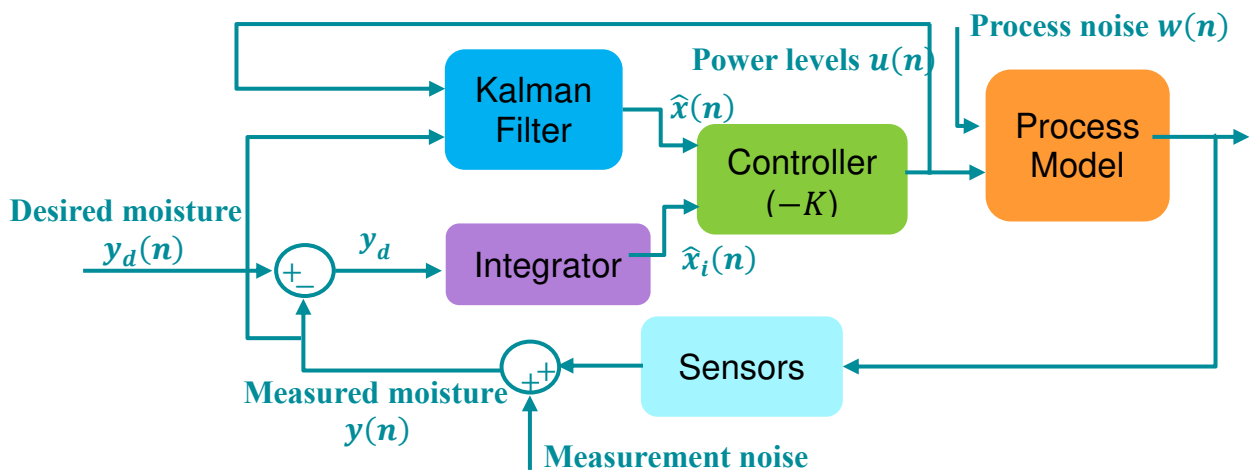


Fig. 24 LQG controller with integral action

TOMOCON				GRANT AGREEMENT No.: 764902	
Deliverable Title: Virtual Controller Structures for TOMOCON Demonstrations					
Del. Rel. No.	EU Del. No.	WP No.	Lead Beneficiary	Type	Date
D4.2.	D13	WP4	ULIB	Report	22.08.2019

4.4. Controller formulation

The microwave drying process is described by coupled Partial Differential Equations (PDEs) which are given in Deliverable 3.2. “Virtual Process Data for Virtual Controller Design”. This system belongs to a class of Distributed Parameter Systems (DPSs) which are characterized by the feature that the state variables, the control variables and/or the system parameters exhibit both spatial and temporal variations.

The PDEs are numerically solved using the Finite Element Method (FEM). Solving the PDEs with this method results in a system of ODEs in which each of them describes the moisture or temperature of the foam at each mesh node. Figure 25 shows the mesh created for the FEM calculations.

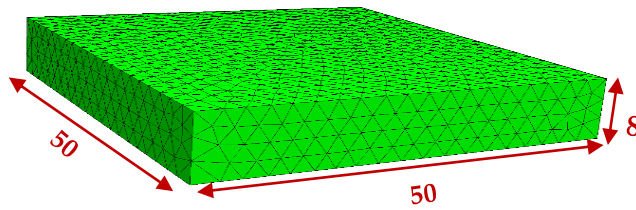


Fig. 25 FEM Mesh for solving PDEs

To design the controller, these ODEs are written in the discrete time state space form as

$$x(n+1) = Ax(n) + Bu(n), \quad (26)$$

where

$$x(n) = [M(n) \quad T(n)]^T \quad (27)$$

$$u(n) = [u_1 \quad u_2 \quad u_3 \quad u_4 \quad u_5 \quad u_6]^T \quad (28)$$

In this form, x is the state vector including the moisture and the temperature at each node, u is a vector indicating the power level of each different microwave source and n refers to time. In the virtual demonstration, there are six microwave sources; however, they can be extended to a greater number of sources in the real demonstration. The dimension of the state vector in this model is twice the number of the mesh nodes. Typically, the DPSs are not controllable in the classical sense. However, the uncontrollable states can be stable and the stability of them can be studied.

As mentioned, the LQG controller is the combination of the LQR controller and the Kalman filter. Each of them can be developed separately. Consider the following state space form:

$$x(n+1) = Ax(n) + Bu(n) + Gw(n), \quad (29)$$

$$y(n) = Cx(n) + Du(n) + v(n), \quad (30)$$

where $y(n)$ is the measured moisture, $w(n)$ and $v(n)$ are the process and measurement noise respectively, and G , C , and D are the corresponding gain matrices. Designing the Kalman filter results in:

$$\hat{x}(n+1|n) = A\hat{x}(n|n-1) + Bu(n) + L[y(n) - C\hat{x}(n|n-1) - Du(n)] \quad (31)$$

TOMOCON				GRANT AGREEMENT No.: 764902	
Deliverable Title: Virtual Controller Structures for TOMOCON Demonstrations					
Del. Rel. No.	EU Del. No.	WP No.	Lead Beneficiary	Type	Date
D4.2.	D13	WP4	ULIB	Report	22.08.2019

where L is the Kalman gain. The estimated states by the Kalman filter should be augmented by the integral of the tracking error as follows:

$$x_i(n+1) = x_i(n) + (y_d(n) - y(n)), \quad (32)$$

$$\bar{x}(n) = [\hat{x}(n) \quad x_i(n)]^T \quad (33)$$

Having the augmented state vector, the LQR controller can be designed. The design procedure involves solving the following optimization

$$\text{Min}_u J = \sum_{n=0}^{\infty} \bar{x}(n)^T Q \bar{x}(n) + u(n)^T R u(n), \quad (34)$$

subject to

$$\bar{x}(n+1) = \bar{A}\bar{x}(n) + \bar{B}u(n) \quad (35)$$

where \bar{A} and \bar{B} are the gain matrices of the augmented system. This results in

$$u(n) = -K \bar{x}(n) \quad (36)$$

where K is the controller gain.

Using a simple model of the microwave drying process in 2D, we have designed the LQR controller with integral action for this process and the results have been studied. It was assumed that all the system states are available and the Kalman filter was not integrated. The controller worked correctly. However, it is just a preliminary result. A more realistic and complete model of the microwave drying process has now been derived. In the next step, the LQG controller with integral action will be designed for the microwave drying process using this model.



TOMOCON				GRANT AGREEMENT No.: 764902	
Deliverable Title: Virtual Controller Structures for TOMOCON Demonstrations					
Del. Rel. No.	EU Del. No.	WP No.	Lead Beneficiary	Type	Date
D4.2.	D13	WP4	ULIB	Report	22.08.2019

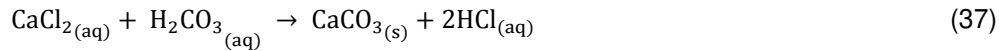
5. Demonstration process: Batch crystallization

5.1. Introduction

The present study describes a mathematical modelling of a lab scale precipitation (crystallization) process and a framework for implementing a PID controller within the MATLAB/Simulink software R2019a. The behavior of a real precipitation system is determined by simultaneous interaction of multiple process phenomena such as spatial and temporal distribution of species concentration (supersaturation), turbulent mixing and overall flow hydrodynamics, which must all be modelled for a comprehensive investigation.

5.2. Physical and computational model

The system of interest is the precipitation process of calcium carbonate (CaCO_3) in a highly alkaline solution at 25 °C. As shown in the reaction equation 37, semibatch precipitation occurs by the addition of different concentrations of high-pH carbonic acid (H_2CO_3) to a calcium chloride (CaCl_2) solution. This is done based on a pre-defined process window, which eventually provides a practical correlation of concentration gradient with mean particle diameter.



Our objective is to establish a series of mathematical equations to describe the semibatch precipitation process. With a semibatch reactor, the amounts of some of the chemical components change by a process other than a reaction, such as the addition of one component to the system. The following sets of equations describe the mole balance applied to an elementary irreversible reaction in semibatch reactors:

$$\frac{dN_{\text{CaCl}_2}}{dt} = r_{\text{CaCl}_2} \cdot V(t) = -\frac{k \cdot N_{\text{CaCl}_2} \cdot N_{\text{H}_2\text{CO}_3}}{V_{t_0} + Q_{\text{inj.}} \cdot t} \quad (38)$$

$$\frac{dN_{\text{H}_2\text{CO}_3}}{dt} = C_{\text{inj.}} \cdot Q_{\text{inj.}} + r_{\text{H}_2\text{CO}_3} \cdot V(t) = C_{\text{inj.}} \cdot Q_{\text{inj.}} - \frac{k \cdot N_{\text{CaCl}_2} \cdot N_{\text{H}_2\text{CO}_3}}{V_{t_0} + Q_{\text{inj.}} \cdot t} \quad (39)$$

$$\frac{dN_{\text{CaCO}_3}}{dt} = r_{\text{CaCO}_3} \cdot V(t) \quad (40)$$

$$\frac{dN_{\text{HCl}}}{dt} = 2 \cdot r_{\text{HCl}} \cdot V(t) \quad (41)$$

Where, $Q_{\text{inj.}}$ is the feed flow rate (m^3/s), $C_{\text{inj.}}$ is the concentration of the reagent in feed solution (mol/m^3), r_i is the reaction rate and is defined as follows

$$r_{\text{CaCl}_2} = r_{\text{H}_2\text{CO}_3} = -k \cdot C_{\text{CaCl}_2} \cdot C_{\text{H}_2\text{CO}_3} \quad (42)$$

$$|r_{\text{CaCl}_2}| = |r_{\text{H}_2\text{CO}_3}| = |r_{\text{CaCO}_3}| = \frac{1}{2} |r_{\text{HCl}}| \quad (43)$$



TOMOCON				GRANT AGREEMENT No.: 764902	
Deliverable Title: Virtual Controller Structures for TOMOCON Demonstrations					
Del. Rel. No.	EU Del. No.	WP No.	Lead Beneficiary	Type	Date
D4.2.	D13	WP4	ULIB	Report	22.08.2019

In equation 42, C_i denotes the concentration of species and k is rate constant. The Arrhenius equation relates the dependence of the rate constant of a chemical reaction on temperature, pre-exponential factor and other constants of the reaction as follows:

$$k = A \cdot \exp\left(-\frac{E}{RT}\right) \quad (44)$$

Where

T is the temperature (in Kelvin),

A is the pre-exponential factor, a constant for each chemical reaction,

E_a is the activation energy for the reaction (in the same units as RT),

R is the universal gas constant ($J/mol \cdot K$)

Change in the solution volume due to the addition of a reagent to the system is calculated by

$$V(t) = V_{t_0} + Q_{inj.} \cdot t \quad (45)$$

The above-mentioned equations are implemented within the Simulink R2019a and the ODE15s solver is selected to solve the set of Ordinary Differential Equations (ODEs). A diagram of graphical blocks is shown in Figure 26. As shown in the figure, concentration distribution (supersaturation) is the final output of the block diagram. Supersaturation distribution inside the reactor acts as a driving force for particle formation and it is directly affected by mixing speed and feed flow rate. The current model does not take into account the effect of flow hydrodynamics and imperfect mixing. Studies are under progress to include an expression that correlates concentration distribution (Figure 32) to flow hydrodynamics, which in turn controls the mean particle size. A simplified method of moments (MOM) as a solution to population balance equation (PBE) is used in order to evaluate the mean particle diameter. Moments from 0 to 3 have physical meanings; each characterizes the total number, length, surface area and volume of particles, respectively. These moments can be obtained by solving the following non-linear ODEs:

$$\frac{d(m_0 V)}{dt} = B_p \cdot V \quad (46)$$

$$\frac{d(m_1 V)}{dt} = m_0 \cdot G \cdot V \quad (47)$$

$$\frac{d(m_2 V)}{dt} = 2m_1 \cdot G \cdot V \quad (48)$$

$$\frac{d(m_3 V)}{dt} = 3m_2 \cdot G \cdot V \quad (49)$$

Where, B_p and G are the primary nucleation rate and growth rate of particles, respectively, and they are defined as power law function of supersaturation:

$$B_p = k_b \cdot \Delta C^b \quad (50)$$

$$G = k_g \cdot \Delta C^g \quad (51)$$

ΔC denotes the supersaturation based on:



TOMOCON				GRANT AGREEMENT No.: 764902	
Deliverable Title: Virtual Controller Structures for TOMOCON Demonstrations					
Del. Rel. No.	EU Del. No.	WP No.	Lead Beneficiary	Type	Date
D4.2.	D13	WP4	ULIB	Report	22.08.2019

$$\Delta C = S = C - C_{equilibrium} = \sqrt{[Ca^{2+}][CO_3^{2-}]} - \sqrt{K_{sp,CaCO_3}} \quad (52)$$

For the current reaction system (equation 37), solubility product constant, $K_{sp,CaCO_3}$, is $10^{-8.48}$. The diagram in Figure 27 displays a block with subsystems that evaluates the mean particle diameter (d_{32}) based on the ratio of fourth and third moments, as follows:

$$d_{32} = \frac{m_3}{m_2} \quad (53)$$

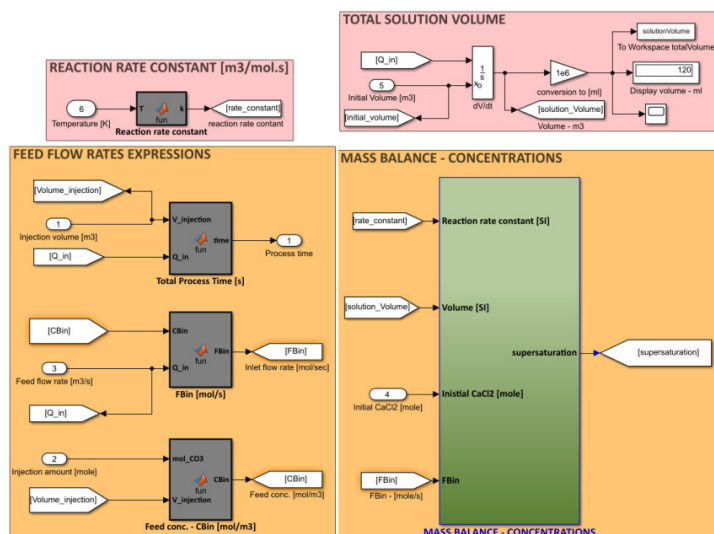


Fig. 26 Block diagram of species mass balance implemented in Simulink

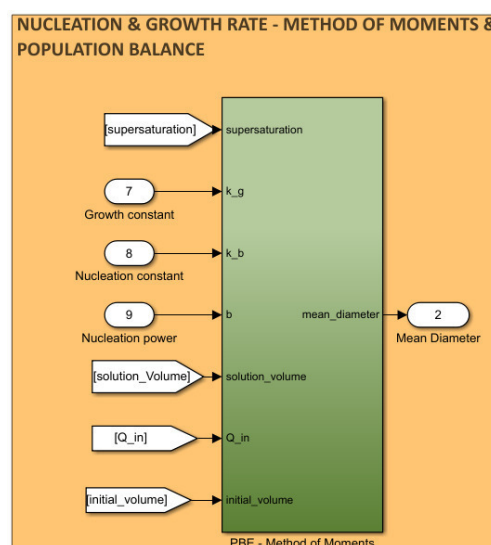


Fig. 27 Block diagram of Moments subsystem in Simulink; output is final process objective

5.3. Tomographic output data in PID controller design

Measuring and controlling a single particle (10-15 microns) with current tomographic technologies is not feasible and practical. However, tomographic measurements (electrical resistance tomography or ultrasound transmission tomography) are able to visualize and quantify the final suspension height (H_s). As shown in a schematic diagram in Figure 28, at various solution volume setpoints during a precipitation process, it is expected that the value of resistance (or transmission) varies due to solution height and settlement of particles.

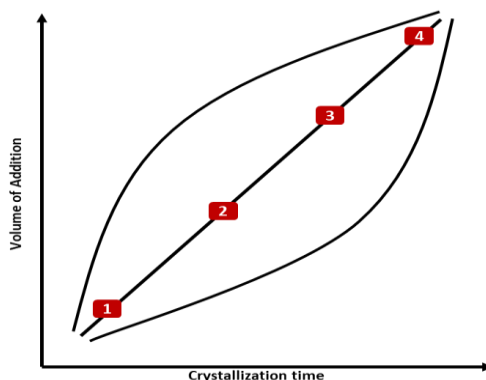


Fig. 28 Tomographic measurement setpoints during a precipitation (crystallization) process

TOMOCON				GRANT AGREEMENT No.: 764902	
Deliverable Title: Virtual Controller Structures for TOMOCON Demonstrations					
Del. Rel. No.	EU Del. No.	WP No.	Lead Beneficiary	Type	Date
D4.2.	D13	WP4	ULIB	Report	22.08.2019

Therefore, our objective is to relate the averaged value of tomographic reconstruction with suspension height and hindered settling velocity (V_t) in order to be used as an input for the PID controller. Based on equation 54, the settling velocity of particles is a function of particle diameter d_p ,

$$d_p = \left(\frac{18\mu V_t}{g(\rho_p - \rho_l)} \right) \quad (54)$$

Where μ is the dynamic viscosity, g is gravitational acceleration, ρ_p and ρ_l are density of particles and liquid, respectively.

5.4. Case study

The following case study demonstrates the behavior of mean particle size to the addition rate of the reagent to the system. The initial reactor volume is at 100 ml and the amount of species (Ca^{2+} and CO_3^{2-}) is set based on a stoichiometric table in a way that at the end of the reaction, all the reactants are consumed. Table 1 tabulates some of the key inputs used in the simulation.

Table 1 Key simulation inputs

Parameter	Amount CO_3^{2-} addition, mole	Amount Ca^{2+} in reactor, mole	Expected $CaCO_3$ precipitation, mole	Volume of addition, ml	Initial volume, ml	Temperature, K	Nucleation rate constant	Growth rate constant
Value	0.02	0.02	0.02	20	100	298.15	9×10^9	5.5×10^{-9}

Figure 29 displays the block diagram of the whole simulation implemented in the Simulink R2019a. Figure 30 shows the volume increase due to the addition of a 20 ml reagent to the system, which results in the precipitation of the target component as shown in Figure 31.

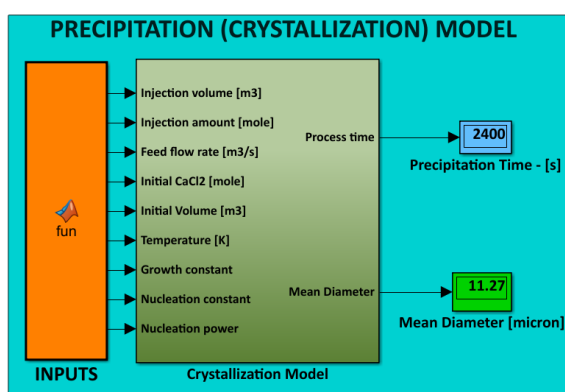


Fig. 29 Overall schematics of the process model implemented in Simulink

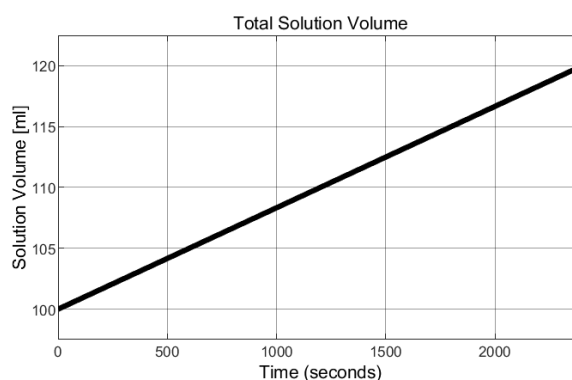


Fig. 30 Solution volume at end of the simulation; 20 ml volume increase from initial amount of 100 ml at a feed rate of 0.5 ml/min

TOMOCON				GRANT AGREEMENT No.: 764902	
Deliverable Title: Virtual Controller Structures for TOMOCON Demonstrations					
Del. Rel. No.	EU Del. No.	WP No.	Lead Beneficiary	Type	Date
D4.2.	D13	WP4	ULIB	Report	22.08.2019

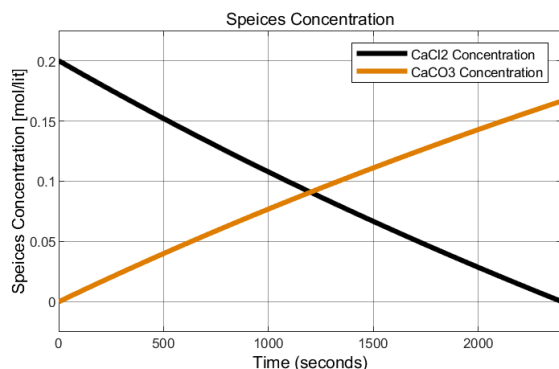


Fig. 31 Species concentration balance

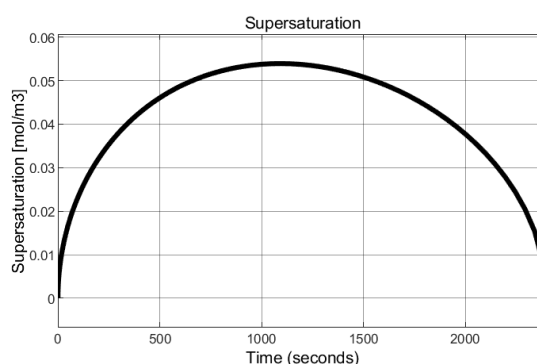


Fig. 32 Supersaturation distribution during the simulation

The results of the simulation and effects of the feed rate on the mean diameter are shown in Table 2. *It must be noted* that as the whole mathematical modelling of the process is at a very initial stage, the current trend of the results is prone to change as the process modelling will get more accurate.

Table 2 Effect of feed flow rate on process output

Feed flow rate (ml/min)	Mean particle diameter (mm)
0.5	11.27
1	56.62
2	90
5	113.6
10	163.1

5.5. Conclusion and future work

The development of a mathematical framework for modelling a precipitation process by utilizing MATLAB/Simulink is described. As the model gets more enhancements by the addition of more critical terms to equations, it can be used for a better prediction of the effects of crucial operating conditions such as feed flow rate on the process output. Figure 33 displays the next step of the work, which is coupling a proportional–integral–derivative (PID) controller to the process model. Eventually, the PID controller through manipulating the key process variable (Feed Flow Rate) evaluates a desired mean particle diameter.

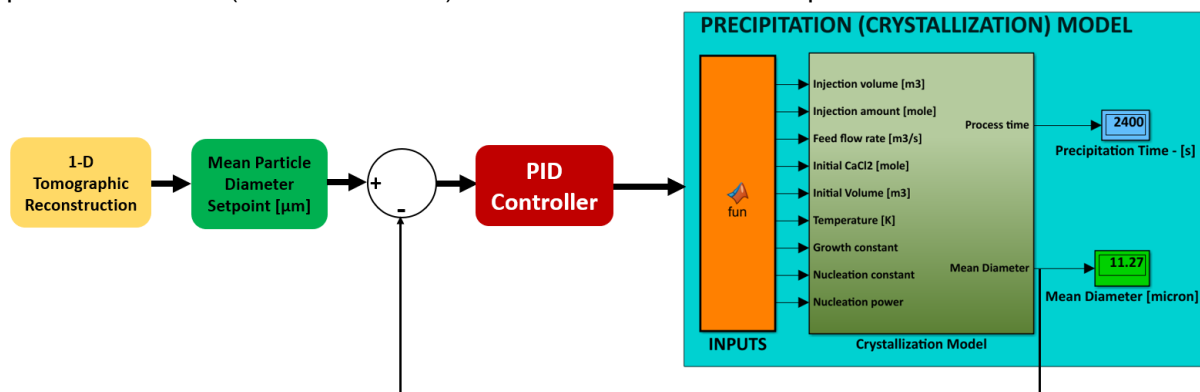


Fig. 33 Final vision of the process model with PID controller

TOMOCON				GRANT AGREEMENT No.: 764902	
Deliverable Title: Virtual Controller Structures for TOMOCON Demonstrations					
Del. Rel. No.	EU Del. No.	WP No.	Lead Beneficiary	Type	Date
D4.2.	D13	WP4	ULIB	Report	22.08.2019

6. Conclusion

Preliminary controller structures have been achieved for all four demonstrations. All of these structures have been implemented as virtual (simulated) controllers using the standard MATLAB/Simulink environment. This environment is very suitable for testing the controllers in their virtual forms. It also has very advanced automatic code generation capabilities and direct support of many embedded hardware platforms. This will significantly streamline and simplify the controller implementation for controlling the real demonstrators in the next stage of the research.

Further, it becomes clear that one of the main challenges of this project is creating models to describe the complex processes in each demonstration. These models must be control oriented i.e. sufficiently accurate but also simple enough to be used for controller design and testing. It is also evident that there is a very close connection between process model structure and controller structure.

For batch crystallization and for inline flow swirl separator; simplified computational fluid dynamics (CFD) models were used to describe the process, where certain physical phenomena were simplified in order to achieve a lumped parameters single input single output model in the end. At this research stage, this model structure allowed the use of PID controllers. However, in the long term these CFD models will need to become more complex to represent the processes more accurately. This might result in the need for more complex controller structures in order to efficiently control these demonstrators.

For the microwave drying process, the partial differential equations needed to describe the process have been space discretized using finite elements method. This results in a set of ordinary differential equations which is then converted to state space form and used to design a LQG controller. This methodology proved to be feasible and implementable in principle. However the state space model that is obtained in this way is of very high order. This very high order implies potential ill conditioning issues with any numerical calculations with state space matrices of this model. This necessitates further studies related to the properties (control loop robustness, controller fragility) of the controller based on this model. Another open question is the use of other model based control approaches, in particular the use of model predictive control.

Lastly, in the case of the continuous casting process modeling based on computational fluid dynamics and partial differential equations turned out to be extremely difficult and unlikely to result in a tractable control oriented model. For this reason, raw data from the UDV or tomography sensors were used and two approaches to their processing were proposed with the objective to obtain suitable numerical characteristics of the continuous casting process. System identification was then applied to the experimental data measured on the Mini-LIMMCAST demonstrator and processed using these two approaches. This resulted in two separate process models. Each of them describes another aspect of the continuous casting process.



TOMOCON				GRANT AGREEMENT No.: 764902	
Deliverable Title: Virtual Controller Structures for TOMOCON Demonstrations					
Del. Rel. No.	EU Del. No.	WP No.	Lead Beneficiary	Type	Date
D4.2.	D13	WP4	ULIB	Report	22.08.2019

From the viewpoint of model structure these models are again single input single output models. However they include several hard constraints that must be respected. This cannot be done using PID control and for this reason model predictive control was used. In order to account for model changes because of process nonlinearity, model predictive control had to be augmented further by using model adaptation and neural network modelling. Further work will need to be done for the process models in order to incorporate more physical information about the process and move towards a grey-box models rather than a black-box models.



TOMOCON				GRANT AGREEMENT No.: 764902	
Deliverable Title: Virtual Controller Structures for TOMOCON Demonstrations					
Del. Rel. No.	EU Del. No.	WP No.	Lead Beneficiary	Type	Date
D4.2.	D13	WP4	ULIB	Report	22.08.2019

7. References

- Ando, T. and Shakouchi, T. Flow Characteristics over forward facing step and through abrupt contraction pipe and drag reduction. Res. Rep. Fac. Eng. Mie Univ., Vol. 29, 2004.
- Bullen, P.R. and Cheeseman, D.J. and Hussain, L.A. A study of turbulent flow in pipe contractions. IMechE, 1996.
- Cho, S.-M. et al. (2012) 'Effect of nozzle clogging on surface flow and vortex formation in the continuous casting mold', Iron and Steel Technology, 9, pp. 85–95.
- Cukierski, K. and Thomas, B. G. (2008) 'Flow Control with Local Electromagnetic Braking in Continuous Casting of Steel Slabs', Metallurgical and Materials Transactions B, 39(1), pp. 94–107.
- Liu, R. et al. (2014) 'Measurements of Molten Steel Surface Velocity and Effect of Stopper-rod Movement on Transient Multiphase Fluid Flow in Continuous Casting', ISIJ International, 54(10), pp. 2314–2323.
- Ren, H. and Wu, Y. Turbulent boundary layers over smooth and rough forward-facing steps. Physics of Fluids 23, 2011.
- Sherry, M. and LoJacono, D. And Sheridan, J. An experimental investigation of the recirculation zone formed downstream of a forward facing step. Journal of Wind Engineering and Industrial Aerodynamics 98, 2010.
- Thomas, B. G. (2003) 'On-line Detection of Quality Problems in Continuous Casting of Steel', p. 16.

